Photocatalytic degradation of reactive blue 21 using ZnO nanoparticles

A.A. El-Bindary[1*], A. Ismail[2], E.F. Eladl[2]

Abstract— Photocatalytic activity of prepared zinc oxide nanoparticles (ZnO) has been investigated using UV light as the energy source. The calculated XRD average crystallite size was found to be 12.24 nm of ZnO. The optical band gap of the sample was found to be 3.21 eV. Optimal experimental conditions on catalysts amount, pH value, illumination time, and dye concentration have been determined. ZnO photocatalyst was characterized for surface area, particle size and crystallinity. The mineralization of RB21 has been confirmed by Chemical Oxygen Demand measurements. Furthermore, the kinetics and scavengers of the reactive species during the degradation were also investigated. It was found that the degradation of RB21 fitted the first-order kinetics and OH• radicals were the main species. Formation of OH• free radicals during irradiation is ascertained by photoluminescence studies using terephthalic acid as probe molecule.

Index Terms— ZnO; Photocatalyst; Reactive blue 21; Kinetics; Fluorescence.

1 Introduction

Organic dyes characterize an important source of environmental contamination, since they are toxic and mostly non-biodegradable [1]. Conventional treatment methods, such as biodegradation, adsorption, flocculation–coagulation, electrocoagulation and conventional chemical oxidation, are not effective enough in achieving total removal of these organic compounds from industrial wastewaters [2,3]. Consequently, different advanced oxidation processes, have been industrial in the last decades in order to improve the oxidation of recalcitrant pollutants, through the generation of highly reactive hydroxyl radicals (•OH) [4-6]. Heterogeneous semiconductor photocatalysis has been recently accessible as a promising technology allowing the total mineralization of different refractory organic compounds, in the presence of either natural or artificial light.

Zinc oxide (ZnO) is one of the most commonly used materials for photocatalytic applications owing to its high chemical stability, low cost, low toxicity, and excellent oxidation properties [7]. As a well-known photocatalyst, zinc oxide possesses a wide band-gap of 3.37 eV and a large exciton binding energy (60 meV). Nevertheless, the low photocatalytic efficiency has been acknowledged as a major obstacle to the degradation of pollutant treatments in large-scale [8]. The semi-conductor properties make this oxide a catalyst for degradation of several recalcitrant substances by using heterogeneous photo-catalysis [9].

Herein, we prepared ZnO nanoparticles using a combination of chemical precipitation and sonochemical methods. After the characterization of the prepared photocatalysts, they used for the degradation of reactive blue 21 (RB21) dye in aqueous solution. A generalized mechanism of chemical reaction of RB21 dye on photocatalysis has also been reported.

2 Materials and Methods

2.1 Materials

Zinc sulfate heptahydrate ($ZnSO_4.7H_2O$) was supplied by Sigma-Aldrich and used as received. A commercial textile dye reactive blue 21 (RB21) was obtained from Cromatos SRL, Italy, and was used without any further purification. A stock solution of RB21 (1.0 g/L) was used, which could be diluted to the required concentration with deionized water in the experiment. All chemical reagents were of analytical grade and used without any further purification. Samples were then conserved in desiccators over anhydrous $CaCl_2$ for further use.

2.2 Preparation of ZnO

ZnO was prepared through co-precipitation-sonochemical processes using deionized water as solvent [5]. A solution of zinc sulfate heptahydrate (0.5 mol, 143.77 g) in 1 L of deionized water was stirred for 30 min. in ultrasonicator. An aqueous solution of ammonia (25%, 100 mL) was added to the previous solution drop by drop with continuous stirring in the ultrasonicator. Then, the ultrasonicator temperature was raised to 60 °C and the solution was agitated by stirring for 30 min. at this temperature. During this period, a solution of sodium bicarbonate (0.3 mol, 25.2 g) as reducing agent was added dropwise. The precipitated $Zn(OH)_2$ was filtered, washed several times by deionized water and dried at 100 °C overnight. Finally, ZnO was obtained by thermal treatment at calcination temperature of 400 °C for 4 hr.

[1]Chemistry Department, Faculty of Science, University of Damietta, Damietta 34517, Egypt.

[2]Environmental Science Department, Faculty of Science, University of Port Said, Port Said, Egypt.
*Corresponding author: E-mail address: abindary@yahoo.com

2.3 Catalyst Characterization

FTIR examination was completed utilizing a JASCO-FT/IR-4100 spectrometer (Jasco, Easton, MD, USA): the finely pounded tests were incorporated into KBr plates before investigation in the wavenumber extend 400–4000 cm^{-1}. The surface morphology of the samples was inspected utilizing scanning electron microscope (SEM) analysis at accelerating voltages of 20 kV (JEOL-JSM-6510 LV). The elemental distribution of ZnO was analyzed using the energy-dispersive X-ray spectroscopy (EDX) and taken on a Leo1430VP microscope with operating voltage 5 kV. Structural variations of the as-prepared materials was investigated by X-ray diffraction (XRD) technique using a Shimadzu XRD-6000 diffractometer (Shimadzu Corporation, Tokyo, Japan) equipped with Cu Kα radiation (λ = 1.54 Å). The 2θ range was varied between 5–80° at a scanning rate of 0.02°. The crystal system, space group and lattice parameters values were considered and optimized using CRYSFIRE and CHEKCELL computer programs [10]. Absorbance measurements of samples were performed on UV-visible spectrophotometer (Perkin-Elmer AA800 spectrophotometer Model AAS) using 1.0 cm quartz cell. Also, Fluorescence Spectrometer (LUMINA, Thermo Scientific) was employed for fluorescence measurements of samples using 1.0 cm quartz cell. Ultrasonic apparatus, Delta 920 (220 V, 300 W, 28 KHz) was used. The isotherm of adsorption/desorption of N_2 on catalyst at 77 K was performed using a Quantachrome Touch Win Instruments version 1.11. curves were analyzed by utilizing Brunauer-Emmett-Teller (BET) method (P/P_o from 0.05 to 0.35) for specific area, t-plot method for external area, volume and area of micropores; and Barrett-Joyner-Halenda (BJH) method for diameter determination of mesopores. HANNA instrument pH meter (model 211) was used for pH modification. HANNA instrument Waste water behavior photometer (model HI 83214) was used for the measurement of chemical oxygen demand (COD).

2.4 Determination of point of zero Charge

The point of zero charge (pH_{PZC}) was resolute by solid addition method [11]. A series of 50 mL (0.1 M) KNO_3 solutions were prepared and their pH values (pH_0) were attuned in the range of 1.0 to 12.0 by addition of 0.1 mol/L HCl and 0.1 mol/L NaOH. To each solution, 0.1 g of catalyst was added and the suspensions were disturbed using shaking water bath at 25 °C. The final pH values of the supernatant were determined (pH_f) after 48 h. The difference between initial (pH_0) and final (pH_f) values ($\Delta pH = pH_0 - pH_f$) (Y-axis) was plotted against the initial pH_0 (X-axis). The intersection of resulting curve yielded the pH_{PZC} where ΔpH = zero.

2.5 Photocatalytic dye degradation experiments

The experimental system for the photodeclorization of 100 mL (40 mg/L, pH = 7.0) aqueous solution RB21 containing 1.0 g/L of the photocatalyst was established in a reactor of a cylindrical Pyrex-glass cell (5 cm inside diameter and 10 cm height) [6]. The suspensions were illuminated under air condition with a medium pressure UV lamp (Philips) which was situated above the reactor (distance 20 cm). The photocatalytic examinations were done under UV irradiation at room temperature using UV lamp: E_{photon} (eV) 3.10–3.94 with λ_{max} (nm) 400–315. The dispersions were sampled out at the structured time intervals during the irradiation process. In order to make certain that adsorption equilibrium between the photocatalyst surface and the RB21 dye took place, the suspensions were magnetically stirred for 30 min (in the dark) before irradiation. Thus, the surface adsorption effect in the removal of RB21 is eradicated. The influence of the initial solution pH was evaluated at different pHs from 2 to 11 (adjusted by HCl (0.1 M) and NaOH (0.1 M)), while RB21 dye concentration was preset at 40 mg/L and 1.0 g/L for the photocatalyst. Photocatalyst dose was changed from 0.2 to 1.8 g/L, for 40 mg/L of RB21 solution, at pH of 7. Also, the effect of the RB21 dye concentration was assessed by varying its concentration from 10 mg/L to 80 mg/L, in the presence of 1.0 g/L of photocatalyst, at a fixed pH of 7. Each sample was withdrawn at a particular time interval and instantly centrifuged at 20,000 rpm for 5 min to remove any dispersed solid catalyst particles for analysis. Finally, the absorbance of RB21 in the supernatant liquid was measured by a UV–visible spectrophotometer, at the maximal absorption wavelength of RB21, λ_{max} = 625 nm. The photodegradation experiments for different Ag/ZnO concentrations (1, 3, 5, 7 and 9%) were performed at 40 mg/L dye concentration, 1.0 g/L catalyst concentration and at pH of 7, to choose one of them to study in details.

The degradation rate (D) of the dye was calculated using Eq. (1):

$$D\ \% = (A_0 - A_t) / A_0 \times 100 \quad (1)$$

Where A_0 represents the initial absorbance of RB21 solution (blank), and A_t is the absorbance after t minutes of irradiation/reaction. According to the Beer–Lambert's law, A_0 and A_t are directly proportional to C_0 and C_t, where C_0 and C_t are the concentrations of blank and sample at (t) time [6].

Chemical oxygen demand (COD) of ZnO before and after photodegradation experiments were measured at regular time intervals. According to the Langmuir–Hinshelwood model, the photodegradation process of pollutants follows the pseudo first-order kinetics, so the photodecolorization rate was studied using Eq. (2):

$$\ln (C_0/C_t) = \ln (A_0/A_t) = kt \quad (2)$$

The optical properties of ZnO were studied by UV-visible absorption spectroscopy at room temperature. The powder samples were dispersed in paraffin oil by sonication then the optical properties were studied at wavelength from 200 nm to 800 nm where paraffin oil was the reference medium.

The photodegradation rate constant k (min^{-1}) was calculated from the slope of the straight-line segment of the plot of ln (C_0/C_t) and the reaction time t as a function of the used experimental parameters.

3 Results and Discussion

3.1 FTIR Analysis

Infrared measurements were performed in order to figure out the purity and nature of ZnO nanoparticles. In general, metal oxides yield absorption peaks at fingerprint region (below 1000 cm^{-1}) as a result of the inter-atomic vibrations. The observed bands at 3440 and 1120 cm^{-1} may arise due to O-H stretching and

deformation respectively which is assigned to the water adsorption on the metal surface [12]. At 1625 cm^{-1}, a relatively less intense band represents the O-H stretching of the adsorbed water molecules. Experimentally, the vibrations of ZnO are in the range of 500–700 cm^{-1}. Bands around 600 cm^{-1} are related to the oxygen deficiency and/or oxygen vacancy deficiency complexes present in ZnO [13].

3.2 X-Ray Diffraction

The XRD analysis was appointed to recognize the phase structure and the purity of the photocatalyst ZnO (Fig. 1). ZnO has the typical hexagonal wurtzite structure with lattice constant a = b = 3.249 Å and c = 5.205 Å (space group P63mc, JCPDS card no. 36-1451) [14]. No additional peaks due to impurities were detected which indicating the high purity of the prepared ZnO. The peaks at 2θ = 31.78, 34.44, 36.25, 47.57, 56.60, 62.87, 67.93, 69.05° can be attributed to (100), (002), (101), (012), (110), (013), (112), (201) planes for ZnO in both samples, respectively [15].

The crystallite size (D, Å) of the ZnO sample was determined by the Scherrer's formula (Eq. 3) [16],

$$D = K\lambda / \beta \cos \theta_B \quad (3)$$

Where, λ is the X-ray wavelength (1.54 Å), β is the angular width of the peak at half of its maximum intensity (full-width at half-maximum) corrected for the instrumental broadening, θ_B is the maximum of the Bragg diffraction peak and K is Scherrer constant (0.9Å). The average crystallite size of ZnO sample was calculated from the first seven peaks and found to be 12.24 nm.

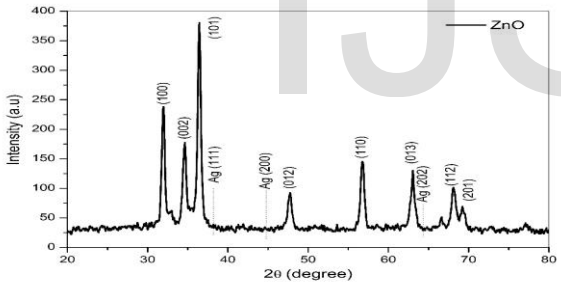

Fig. 1. XRD patterns of pure ZnO and Ag/ZnO (3%) photocatalysts.

3.3 Scanning electron microscope (SEM) analysis

In order to investigate the surface morphology, size, shape and growth mechanism of ZnO nanoparticles, SEM analysis was performed (Fig. 2). From the SEM image, nanoparticles seem to be nearly spherical, closely packed and randomly oriented [5]. Pure ZnO powder consists of nanoparticles with an average size of about 33 nm.

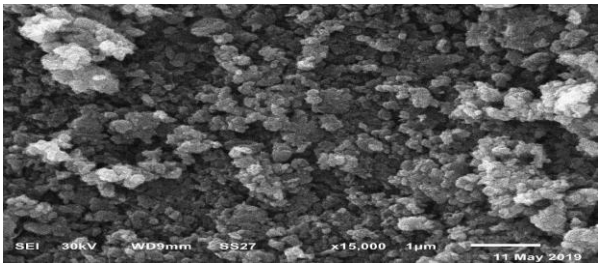

Fig. 2. SEM image of ZnO.

3.4 Energy dispersive X-ray (EDX) analysis

The evaluation using energy dispersive X-ray analysis is based on the concept of providing unique set of peaks on X-ray spectrum for each element in unique atomic structure. The elemental composition of both ZnO nanostructures were estimated by EDX analysis coupled with SEM. In the ZnO diagram, the peaks of Zn and O are set up without the detection of peaks for impurities (Fig. 3).

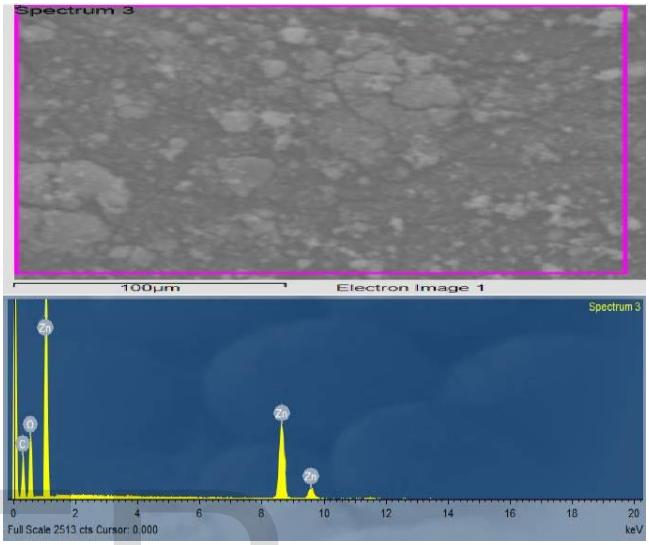

Fig. 3. EDX spectrum of ZnO.

3.5 Optical band gap energy (Eg)

The quantity of the energy band gap of ZnO nanostructures has been determined by studying of the optical properties of these particles using UV-visible spectroscopy. The band gap energy was determined using Tauc's formula [17] which shows the relationship among absorption coefficient as follows (Eq. 4):

$$(\alpha h\upsilon)^{1/n} = B(h\upsilon - E_g) \quad (4)$$

Where α is the absorption coefficient, h is Planck's constant and υ is the frequency ($\upsilon = c/\lambda$, λ is the wavelength, c is the light speed). Exponent n depends on the type of transition and it may have values 1/2, 2, 3/2 and 3 corresponding to the allowed direct, allowed indirect, forbidden direct and forbidden indirect transitions, respectively [18]. B is a constant and generally called band tailing parameter. Thus, the band gap energy was obtained graphically from $(\alpha h\upsilon)^2$ *vs.* $h\upsilon$ for direct transition, extrapolating the linear part on the abscissa according to Eq. 4. The band gap energy was found to be 3.21 eV at 386 nm [4].

3.6 Brunauer-Emmett-Teller (BET) surface area

The Brunauer-Emmett-Teller (BET) [19] surface area and Barrett-Joyner-Halenda (BJH) pore size of ZnO have been estimated using N_2 adsorption/desorption measurements at 77 K (Fig. 4). The N_2 adsorption-desorption isotherms of ZnO and nanoparticles are assorted as type II that pointed to non-porous solid at P/P_o = 0.99. The isotherm is completely reversible without any hysteresis loop enlightening the absence of any pore type which could allow capillary condensation process. The specific surface area was calculated by BET equation in its normal range of applicability and adopting a value of 16.2 Å for the cross-section

area of N_2 molecule and it was found to be 7.643 m^2/g for ZnO. Though, the total pore volume at saturation pressure and expressed as liquid volume were found 0.092 and 0.157 cm^3/g for ZnO. As well as the pore radii was calculated by BJH pore size distribution curve and was found to be 2.201 nm [5].

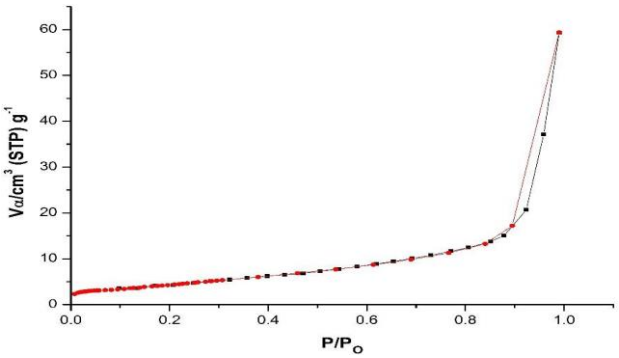

Fig. 4. Sorption isotherm of ZnO collected by N_2 adsorption/desorption experiment at 77 K.

3.7 Determination of point of zero charge (pH_{PZC})

Surface charge of commercial ZnO was determined by the PZC, which is defined as the pH (pH_{PZC}) at which the positive charges on the surface equal the negative charges [11]. The pH_{PZC} of ZnO was found to be 7.4. This shows that below this pH, the ZnO acquires a positive charge owing to protonation of functional groups and above this pH, negative charge exists on the surface.

3.8 Effect of Operating Parameters on the Photocatalytic degradation of RB21

3.8.1 Effect of initial dye concentration

The influence of preliminary dye concentration on its degradation has been studied with different concentrations of RB21 from 10 to 80 mg/L with a constant concentration of the ZnO catalyst at 0.6 g/L. Results summary for both catalysts on degradation rates of RB21 after reaction time of 30 min. are shown in (Fig. 5). It is generally noted that the degradation rate of low initial concentrations of RB21 (up to 40 mg/L) is more than that of the higher initial concentrations [20]. As a result, it is expected that increasing the initial concentration of RB21 will increase the probability of reaction between RB21 molecules and oxidizing species which will lead to an improvement in the degradation rate [21].

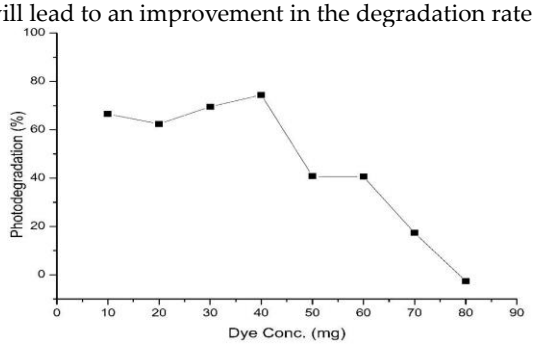

Fig. 5. Effect of initial dye concentration on the photodegradation activity of ZnO photocatalyst (dosage 1.0 g/L and pH = 7) under UV irradiation time for 30 min.

3.8.2 Effect of photocatalyt dosage

The effect of the catalyst concentration on the photodegradation efficiency of the process was estimated in the range of 0.2–1.8 g/L keeping RB21 dye concentration constant at 40 mg/L. The photodegradation rate of RB21 grows up with increasing the photocatalyst dosage (to the optimum value 1.0 g/L for ZnO) and then goes down. The more the photocatalyst amount, the more the active sites are found on the photocatalyst surface, which leads to promotion of hydroxyl radical formation [5]. However, over increase in the amount of the catalyst has a negative effect, because of the screening effect of the aggregation of catalyst particles which can prevent photons to get to inner surface of the catalyst [6].

3.8.3 Effect of pH

The medium pH is an important in operation variable that used in the determination the efficiency of the photocatalytic removal of different pollutants in wastewaters. The effect of changing pH from 2 to 11 for the initial RB21 solution is shown in Fig. 6, for an initial RB21 concentration of 40 mg/L, over ZnO photoctalyst (1.0 g/L), and under UV irradiation. Photocatalytic degradation efficiency decreases with a further raise in pH, showing that the initial pH of the dye solution affects the adsorption of the organic compound on the photocatalyst surface and expresses an important step in the overall reaction mechanism of dye oxidation [22].

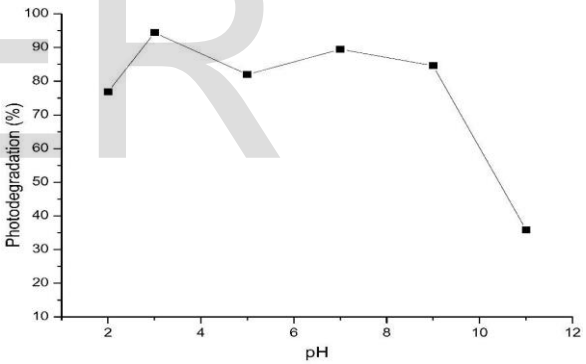

Fig. 6. Effect of pH on the properties of ZnO photocatalyst (40 mg/L dye concentration and dosage 1.0 g/L) under UV irradiation time for 30 min.

Though, a further raise in pH is responsible for an increase in coulombic repulsion between the negatively charged ZnO surface and the OH^- species included in the photocatalytic oxidation mechanism, principal to decreased degradation efficiency. In addition, in the acidic conditions, the structure of the dye might be changed into the quinoid structure, which is unstable and could be easily destroyed [23].

3.9 Estimation of chemical oxygen demand (COD)

To measure the organic strength of wastewater, the chemical oxygen demand (COD) is widely used as an effective technique [24]. The test allowed the measurement of waste in terms of the total quantity of oxygen required for oxidation of organic matter to CO_2 and H_2O. Chemical oxygen demand (COD) was used to examine the photodecolorization of the dye [25]. The COD of the dye solution before and after the treatment was estimated. Chem-

ical oxygen demand was measured after exposure the sample to UV irradiations at times 0, 30, 60 min to check the photodecolorization of RB21 dye and found to be 225, 100, 40 ppm, respectively. The observed decrease in the COD values of the preserved dye solution with increasing time indicating the complete mineralization of dye into non-toxic species.

3.10 Degradation Kinetics

The photodegradation rate of RB21 dye on 1.0 g/L of ZnO photocatalyst was evaluated under UV irradiation (Fig. 7). Normally, photocatalytic processes are performed only in water because the radicals can only react with the dye dissociated. A pseudo-first-order kinetics equation was used to estimate the kinetic rate constant (k) value for the photodegradation process of RB21 onto the photocatalysts surface and are expressed using Eq. (2). The kinetic constant was determined by the analytical integration method. The linear relationship between $\ln(C_0/C_t)$ and the reaction time *t* of RB21 dye follows a pseudo-first-order kinetics functioning with correlation coefficient (R^2= 0.9887 and 0.9854) [26]. The photocatalytic reaction follows a pseudo-first-order reaction; the corresponding apparent rate constant (k) is estimated to be $1.99x10^{-2}$ min^{-1} (Fig. 7) [27].

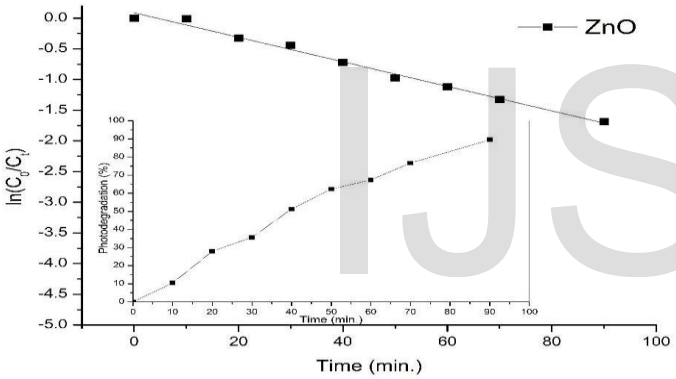

Fig. 7. Photocatalytic degradation kinetic curves of RB21 over ZnO under UV irradiation (40 mg/L dye concentration, dosage 1.0 g/L and pH = 7).

3.11 Stability of Photocatalyst ZnO

The stability of the prepared photocatalyst ZnO was investigated by recycling experiments of the photocatalytic degradation of RB21 in the presence of UV irradiation. In this experiment, the photocatalyst was separated from the sample and collected after each cycle by centrifugation, then washed with both distilled water and ethanol and dried in an oven at 100 °C. The sample was then reused for subsequent degradation. As can be seen, the efficiency of the degradation of RB21 after 90 min decreased from 89.78 to 84.76 after three cycles. Similarly, the photocatalytic activity of the samples only minimally decreases, due to the unavoidable loss of photocatalyst during the cycle processes.

3.12 Mechanism of photodegradation

The surface area and crystal structure are the responsible of that effect, but also other factors such as band gap energy, oxidation state of the dopant, and recombination of the photogenerated electron–hole pairs may be taken in the consideration for ZnO [28]. To understand the mechanism of the degradation of RB21 on ZnO, it is important to indicate which of these reactive species plays the essential role the photocatalytic degradation process. The photodegradation of RB21 over ZnO was studied using silver nitrate (e− scavenger), potassium iodide (h+ scavenger) and isopropanol ($OH^\bullet$ scavenger) in the reaction solution [29].

When the photocatalyst (ZnO) is irradiated with photons (hυ) of energy equal to or more than its band gap energy (3.36 eV), some electrons (e^-) of the valence band (VB) are excited and jump to the conduction band (CB) which leaves behind equivalent holes (h^+) in the VB:

$$ZnO + h\upsilon \rightarrow ZnO\,(h^+_{(VB)}) + ZnO\,(e^-_{(CB)}) \quad (5)$$

Where hυ is the energy required to transfer an electron from valence band to conduction band. In this photoexcited state, electrons can reduce dissolving oxygen to generate superoxide radical anions ($O_2^{\bullet-}$), whereas the photoexcited holes in VB have the ability to oxidize hydroxyl anions (OH^-) and H_2O to produce hydroxyl radicals ($OH^\bullet$). After the formation these highly active radicals, they can destroy dye molecules and generate the small molecules CO_2 and H_2O.

$$e^-_{(CB)} + O_2 \rightarrow O_2^{\bullet-} \quad (6)$$

$$O_2^{\bullet-} + H_2O \rightarrow HO_2^\bullet + OH^\bullet \quad (7)$$

At the same time, the photoinduced holes could be trapped by the hydroxyl groups (or H_2O) on the photocatalyst surface to produce hydroxyl radicals ($OH^\bullet$) [30]:

$$OH^- + h^+_{(VB)} \rightarrow OH^\bullet \quad (8)$$

$$H_2O \leftrightarrow (H^+ + OH^-) + h^+_{(VB)} \rightarrow OH^\bullet + H^+ \quad (9)$$

At the final stage, these highly active radicals have the ability to degrade the dye molecules (RB21) to yield carbon dioxide and water as follows:

$$OH^\bullet + RB21 + O_2 \rightarrow \text{products } (CO_2 \text{ and } H_2O) \quad (10)$$

In the meantime, these photoinduced holes and electrons can recombine to lessen the efficiency of photodegradation. However, the addition of noble metals to the semiconductor photocatalyst can inhibit this recombination [31]:

$$ZnO\,(h^+_{(VB)}) + ZnO\,(e^-_{(CB)}) \rightarrow ZnO \quad (11)$$

Creation of $OH^\bullet$ free radicals is established by means of photoluminescence studies using terephthalic Acid (TPA) as a probe molecule. TPA reacts with $OH^\bullet$ free radicals to yield 2-hydroxyterphthalic acid which shows a characteristic luminescence peak at 420 nm [32]. The intense luminescence peak at 420 nm for sample containing ZnO + TPA after irradiation for 20, 40, 60, 80 and 100 min clearly shows the presence of $OH^\bullet$ free radicals during irradiation (Fig. 8).

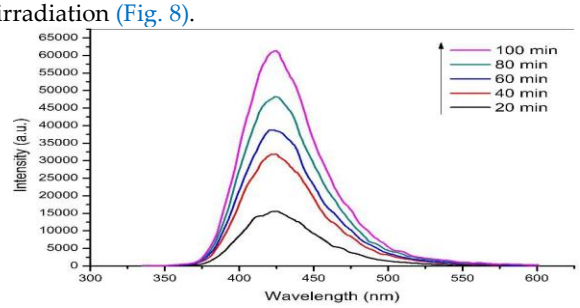

Fig. 8. Photoluminescence spectra of ZnO+TPA after irradiation (40 mg/L initial dye concentration, 1.0 g/L ZnO, $4.8x10^{-4}$ M terephthalic acid and pH =7).

4 Conclusion

Photocatalytic activity of commercial ZnO photocatalyst was examined for the treatment of aqueous solutions containing RB21 under UV light irradiation. The catalyst was characterized by different spectroscopic techniques. Optical measurements indicated that the band gap value of ZnO was found to be 3.21. The effect of operation parameters such as pH, catalyst dosage, and initial dye concentration was estimated. It was found that the degradation of RB21 fitted the first-order kinetics and $OH^{\bullet}$ radicals were the main species. Formation of $OH^{\bullet}$ free radicals during irradiation is ascertained by photoluminescence studies using terephthalic acid as probe molecule. The degradation extent was checked by UV-vis spectroscopy and confirmed by chemical oxygen demand.

References

[1] J.E.B. McCallum, S.A. Madison, S. Alkan, R.L. Depinto, R.U.R. Wahl, Analytical studies on the oxidative degradation of the reactive textile dye uniblue A, *Environ. Sci. Technol*. 2000, 34, 5157.

[2] A. Hassani, L. Alidokht, A.R. Khataee, S. Karaca, Optimization of comparative removal of two structurally different basic dyes using coal as a low-cost and available adsorbent, *J. Taiwan Inst. Chem. Eng.* 2014, 45, 1597.

[3] C.B. Ong, L.Y. Ng, A. Mohammad, A review of ZnO nanoparticles as solar photocatalysts: Synthesis, mechanisms and applications, *Renew. Sustain. Energy Rev.*, 81 (2018) 536-551.

[4] A.A. El-Bindary, S.M. El-Marsafy, A.A. El-Maddah, Enhancement of the photocatalytic activity of ZnO nanoparticles by silver doping for the degradation of AY99 contaminants, *J. Mol. Struct*. 1191 (2019) 76–84.

[5] H.A. Kiwaan, T.M. Atwee, E.A. Azab, A.A. El-Bindary, Efficient photocatalytic degradation of acid red 57 using synthesized ZnO nanowires, *J. Chin. Chem. Soc*. 66 (2019) 89–98.

[6] H.A. Kiwaan, T.M. Atwee, E.A. Azab, A.A. El-Bindary, Photocatalytic degradation of organic dyes in the presence of nanostructured titanium dioxide, *J. Mol. Struct*. 1200 (2020) 127115.

[7] I.J. Ani, U.G. Akpan, M.A. Olutoye, B.H. Hameed, Photocatalytic degradation of pollutants in petroleum refinery wastewater by TiO_2- and ZnO-based photocatalysts: Recent development, *J. Clean. Prod.*, 205 (2018) 930-954.

[8] S. Bhatia, N. Verma, Photocatalytic activity of ZnO nanoparticles with optimization of defects, *Mater. Res. Bull.*, 95 (2017) 468-476.

[9] K.M. Lee, C.W. Lai, K.S. Ngai, J.C. Juan, Recent developments of zinc oxide based photocatalyst in water treatment technology: A review, *Water Research*, 88 (2016) 428-448.

[10] R. Shirley, The CRYSFIRE System for Automatic Powder Indexing: User's Manual, The Lattice Press, 41 Guildford Park Avenue, Guildford, Surrey GU2 7NL, England, 2000.

[11] K.Z. Elwakeel, A.A. El-Bindary, E.Y. Kouta, E. Guibal, Functionalization of polyacrylonitrile/Na-Y-zeolite composite with amidoxime groups for the sorption of Cu(II), Cd(II) and Pb(II) metal ions, *Chem. Eng. J.*, 332 (2018) 727-736.

[12] A.R. Prasad, P. Rugmini Ammal, A. Joseph, Effective photocatalytic removal of different dye stuffs using green synthesized zinc oxide nanogranules, *Mater. Res. Bull.*, 102 (2018) 116-121.

[13] G. Xiong, U. Pal, J.G. Serrano, K.B. Ucer, R.T. Williams, Photoluminesence and FTIR study of ZnO nanoparticles: the impurity and defect perspective, *Phys. Stat. Sol*., 3 (2006) 3577–3581.

[14] K. Omri, I. Najeh, R. Dhahri, J. El Ghoul, L. El Mir, Effects of temperature on the optical and electrical properties of ZnO nanoparticles synthesized by sol–gel method, *Microelect. Eng*., 128 (2014) 53-58.

[15] R. Krithiga, G. Chandrasekaran, Synthesis, strucutral and optical properties of vanadium doped zinc oxide nanograins, *J. Cryst. Growth*, 311 (2009) 4610-4614.

[16] A.L. Patterson, The Scherrer formula for X-Ray particle size determination, *Phys. Rev*., 56 (1939) 978-982.

[17] J. Tauc, R. Grigorovici, A. Vancu, Optical properties and electronic structure of amorphous germanium, *Phys. Status Solidi*, 15 (1966) 627-637.

[18] A.A. Essawy, Silver imprinted zinc oxide nanoparticles: green synthetic approach, characterization and efficient sunlight-induced photocatalytic water detoxification, *J. Clean. Prod*., 183 (2018) 1011-1020.

[19] S. Brunauer S., Emmett P.H., Teller E., Adsorption of gases in multimolecular layers, *J. Am. Chem. Soc*., 60 (1938) 309-319.

[20] Y. Ni, D. Jiang, Y. Gao, X. Zhu, H. Zhang, Raspberry-like monodispersity ZnO microspheres for photodegradation of rhodamine B, *Mater. Res. Bull*., 99 (2018) 37-44.

[21] L. Saikia, D. Bhuyana, M. Saikia, B. Malakar, D.K. Dutta, P. Sengupta, Photocatalytic performance of ZnO nanomaterials for self sensitized degradation of malachite green dye under solar light, *Appl. Catal. A Gen*., 490 (2015) 42–49.

[22] V. Kuzhalosai, B. Subash, A. Senthilraja, P. Dhatshanamurthi, M. Shanthi, Synthesis, characterization and photocatalytic properties of SnO2-ZnO composite under UV-A light, *Spectrochim. Acta A*, 115 (2013) 876–888.

[23] A. Jain, A. Ashma, K. Marazban, Expedient degradation of dye methyl green by enhanced photo--fenton process: a green chemical approach, *J. Appl. Chem*., 2 (2014) 13–25.

[24] M.C. Hasegawa, J.F. Daniel, K. Takashima, G.A. Batista, S.M. da Silva, COD removal and toxicity decrease from tannery wastewater by zinc oxide-assisted photocatalysis: a case study, *Environ. Technol*., 35 (2014) 1589-1595.

[25] [46] M.Y. Ghalya, J.Y. Faraha, A.M. Fathy, Enhancement of decolorization rate and COD removal from dyes containing wastewater by the addition of hydrogen peroxide under solar photocatalytic oxidation, *Desalination*, 217 (2007) 74-84.

[26] G. Crini, Kinetics and equilibrium studies on the removal of cationic dyes from aqueous solution by adsorption onto a cyclodextrin polymer, *Dyes Pigments*, 77 (2008) 415-426.

[27] F.C. Wu, R.L. Tseng, R.S. Juang, Kinetic modeling of liquid-phase adsorption of reactive dyes and metal ions on chitosan, *Water Res*., 35 (2001) 613-618.

[28] E. Topkaya, M. Konyar, H.C. Yatmaz, K. Ozturk, Pure ZnO and composite ZnO/TiO2 catalyst plates: a comparative study for the degradation of azo dye, pesticide and antibiotic in aqueous solutions, *J. Colloid Interf. Sci*., 430 (2014) 6-11.

[29] N. Huang, J. Shu, Z. Wang, M. Chen, C. Ren, W. Zhang, One-step pyrolytic synthesis of ZnO nanorods with enhanced photocatalytic activity and high photostability under visible light and UV light irradiation, *J. Alloy. Comp*., 648 (2015) 919-929.

[30] X. Chen, Z. Wu, D. Liu, Z. Gao, Preparation of ZnO photocatalyst for the efficient and rapid photocatalytic degradation of azo dyes, *Nanoscale Res. Lett*., 12 (2017) 143-152.

[31] A. Houas, H. Lachheb, M. Ksibi, E. Elaloui, C. Guillard, J.M. Herrmann, Photocatalytic degradation pathway of methylene blue in water, *Appl. Catal. B Environ*., 31 (2001) 145-157.

[32] L. Saikia, D. Bhuyan, M. Saikia, B. Malakar, D.K. Dutta, P. Sengupta, Photocatalytic performance of ZnO nanomaterials for self-sensitized degradation of malachite green dye uder solar light, *Appl. Catal. Gen*., 490 (2015) 42-492-49.